Ultrafast phase and amplitude pulse shaping with a single, one-dimensional, high-resolution phase mask.

Jesse W. Wilson, Philip Schlup, and Randy A. Bartels*

Electrical and Computer Engineering Department, Colorado State University, 1320 Campus Delivery, Fort Collins, CO 80523, USA

**Corresponding author: bartels@engr.colostate.edu*

Abstract: An ultrafast pulse shaper, capable of both phase and amplitude shaping, is constructed using a single high-resolution liquid crystal phase mask. The shaper is calibrated with an inline spectral interferometry technique. Amplitude shaping is accomplished by writing to the mask a phase grating, whose period is smaller than the spectral focus, diffracting away selected frequencies in a controllable manner.

OCIS codes: (230.3720) Liquid-crystal devices; (230.6120) Spatial light modulators; (320.5540) Ultrafast Pulse shaping

References and links

1. A. M. Weiner, "Femtosecond pulse shaping using spatial light modulators," Rev. Sci. Instrum. **71**, 1929–1960 (2000).
2. R. Bartels, S. Backus, E. Zeek, L. Misoguti, G. Vdovin, I. P. Christov, M. M. Murnane, and H. C. Kapteyn, "Shaped-pulse optimization of coherent emission of high-harmonic soft X-rays," Nature (London) **406**, 164–166 (2000).
3. A. Assion, T. Baumert, M. Bergt, T. Brixner, B. Kiefer, V. Seyfried, M. Strehle, and G. Gerber, "Control of chemical reactions by feedback-optimized phase-shaped femtosecond laser pulses," Science **282**, 919–922 (1998).
4. M. M. Wefers and K. A. Nelson, "Analysis of Programmable Ultrashort Wave-Form Generation Using Liquid-Crystal Spatial Light Modulators," J. Opt. Soc. Am. B **12**, 1343–1362 (1995).
5. C. W. Hillegas, J. X. Tull, D. Goswami, D. Strickland, and W. S. Warren, "Femtosecond Laser-Pulse Shaping by Use of Microsecond Radiofrequency Pulses," Opt. Lett. **19**, 737–739 (1994).
6. J. C. Vaughan, T. Hornung, T. Feurer, and K. A. Nelson, "Diffraction-based femtosecond pulse shaping with a two-dimensional spatial light modulator," Opt. Lett. **30**, 323–325 (2005).
7. F. Verluise, V. Laude, Z. Cheng, C. Spielmann, and P. Tournois, "Amplitude and phase control of ultrashort pulses by use of an acousto-optic programmable dispersive filter: pulse compression and shaping," Opt. Lett. **25**, 575–577 (2000).
8. E. Frumker, E. Tal, Y. Silberberg, and D. Majer, "Femtosecond pulse-shape modulation at nanosecond rates," Opt. Lett. **30**, 2796–2798 (2005).
9. V. Bagnoud and J. D. Zuegel, "Independent phase and amplitude control of a laser beam by use of a single-phase-only spatial light modulator," Opt. Lett. **29**, 295–297 (2004).
10. M. A. Dugan, J. X. Tull, and W. S. Warren, "High-resolution acousto-optic shaping of unamplified and amplified femtosecond laser pulses," J. Opt. Soc. Am. B **14**, 2348–2358 (1997).
11. T. Binhammer, E. Rittweger, R. Ell, F. X. Kartner, and U. Morgner, "Prism-based pulse shaper for octave spanning spectra," IEEE J. Quantum Electron. **41**, 1552–1557 (2005).
12. A. M. Weiner, "Femtosecond Optical Pulse Shaping and Processing," Prog. Quantum Electron. **19**, 161–237 (1995).
13. S. Akturk, X. Gu, M. Kimmel, and R. Trebino, "Extremely simple single-prism ultrashort-pulse compressor," Opt. Express **14**, 10,101–10,108 (2006).
14. D. J. Kane and R. Trebino, "Characterization of Arbitrary Femtosecond Pulses Using Frequency-Resolved Optical Gating," IEEE J. Quantum Electron. **29**, 571–579 (1993).

#84226 - $15.00 USD Received 20 Jun 2007; revised 28 Jun 2007; accepted 29 Jun 2007; published 5 Jul 2007

15. D. J. Kane, "Real-time measurement of ultrashort laser pulses using principal component generalized projections," IEEE J. Sel. Top. Quantum Electron. **4**, 278–284 (1998).
16. P. Schlup, J. Wilson, K. Hartinger, and R. A. Bartels, "Dispersion-balancing of variable-delay monolithic pulse-splitters," To be published in Appl. Opt. (2007).
17. M. Takeda, H. Ina, and S. Kobayashi, "Fourier-Transform Method of Fringe-Pattern Analysis for Computer-Based Topography and Interferometry," J. Opt. Soc. Am. **72**, 156–160 (1982).

1. Introduction

Programmable ultrafast optical pulse shapers are ubiquitous, with applications ranging from simple dispersion control to carefully shaped laser pulses used for coherent control of quantum dynamics [1, 2, 3]. While many applications utilize spectral phase-only shaping for simplicity, one also needs control over amplitude to access a complete range of temporal shapes, e.g. square and sinc pulses. Such control in the standard zero-dispersion Martinez stretcher has been implemented with pairs of liquid crystal spatial light modulators (LC-SLMs) [4], volume Bragg gratings written with an acousto-optic modulator (AOM) crystal [5], and recently by a two-dimensional (2D) LC-SLM with a blazed phase grating in the direction lacking spectral dispersion [6]. A complementary technology, acousto-optic programmable dispersion filters (AOPDFs) [7], also provides spectral phase and amplitude control.

Here we introduce a new approach to phase and amplitude pulse shaping with a folded Martinez stretcher and a *single*, linear, high-resolution LC-SLM. Typically, when one designs a pulse shaper employing a LC-SLM, the spatial mode in the Fourier plane is matched to the pixel size of the SLM in order to optimize the spectral resolution. In our device, the spatial mode includes a large number of SLM pixels, effectively oversampling the spatial mode [8]. This permits spectral amplitude shaping via a high spatial-frequency sinusoidal phase grating. We utilize diffraction from this phase grating to scatter intensity from selected frequency components to higher orders, collecting the zero-order beam to reconstruct a shaped pulse. As a result, the maximum throughput is attained by switching off the phase grating. Complete spectral attenuation is in principle possible by the appropriate choice of phase grating depth of modulation. This contrasts with 2D phase–amplitude shaping [6], where the blazed grating written onto the SLM must be carefully optimized to obtain efficient diffraction into the output beam of the shaper, even in the absence of spectral amplitude shaping. The use of phase-only LC-SLMs to generate phase gratings is not limited to ultrafast pulse shaping: control over spatial mode phase and amplitude has been reported, using a 2D LC-SLM and phase gratings [9].

Though diffractive effects have long been used in AOM devices to shape both spectral phase and amplitude [5], the approach presented here differs significantly from AOM shaping. Acousto-optic shapers operate through Bragg diffraction of the incident light at the Fourier plane, reconstructing the first-order diffracted beam into a shaped pulse. Thus the acousto-optic device throughput is fundamentally limited by the first-order diffraction efficiency, reported to be $\sim 50\%$ at 620 nm in an experimental device [5]. The optical bandwidth of AOM shapers is limited to a single octave, since beyond this higher order diffracted beams will overlap [10]. AOMs can be rapidly reconfigured between pulses, but the finite acoustic wave velocity places an upper limit on the repetition rate of shaped pulses [8]. While this is well-suited for amplified pulses, a pulse picker must be employed in the typical cases of multi–MHz ultrafast oscillator pulse trains.

Our approach can be used with octave-spanning optical bandwidths by employing a prism as the dispersive element [11], as the overlapping diffracted orders from the phase grating are discarded. In addition, the LC-SLM phase masks can remain static from one pulse to another, allowing for operation with oscillator pulse trains without the use of a pulse picker. The masks can typically be changed in ~ 30 ms. Combined with the high optical reflectivity of the LC-SLM (greater than 90%), these aspects make this technique especially attractive for nonlinear

#84226 - $15.00 USD Received 20 Jun 2007; revised 28 Jun 2007; accepted 29 Jun 2007; published 5 Jul 2007

optical experiments with an oscillator and octave-spanning supercontinuum spectra.

1.1. Simultaneous phase and amplitude shaping

To understand this approach mathematically, we employ notation for pulse shaper analysis following Ref. [12]. The pulse just after the masking plane is

$$E_{\text{in}}(\omega)e^{(x-\alpha\omega)^2/w_0^2}M(x), \tag{1}$$

where $E_{\text{in}}(\omega)$ is the Fourier transform of the incident pulse, w_0 is the $1/e^2$ intensity radius of the focused beam, and α is set by the angular dispersion and focal length of the stretcher. Next we apply a high-resolution phase-only mask,

$$M(x) = \exp\left[i\Delta(x)\sin(2\pi f_g x) + i\phi(x)\right], \tag{2}$$

a superposition of a sinusoidal phase grating with spatial frequency f_g and depth of modulation Δ, and a slow additional phase ϕ. Expanding this sinusoidal phase into a series of Bessel functions, we find that if f_g is sufficiently high, the shaper optics only collect the zero order and convert the phase grating to amplitude control:

$$M(x) \approx J_0\left[\Delta(x)\right]\exp\left[i\phi(x)\right]. \tag{3}$$

From this result, we expect full spectral amplitude control from a high frequency sinusoidal phase grating, by adjusting $\Delta(x)$ to modulate spatial diffraction across the spectrum dispersed in the Fourier plane. Spectral phase control is imparted by adding the appropriate slow phase value $\phi(x)$.

1.2. Setup

We demonstrate the efficacy of this technique with two implementations of the pulse shaper: one with a prism for low angular dispersion, potentially applicable to octave-spanning spectra; the other with a grating for high angular dispersion. In both cases, the dispersive element is placed at the front focal plane of a convex lens and the reflective SLM is placed at the back focal plane. The phase mask we use is a $1\times$12,288 Linear Series spatial light modulator provided by Boulder Nonlinear Systems (Lafayette, CO). The liquid crystal elements have a 1.6 μm pixel pitch, comprising a 1.0 μm transmissive electrode and a 0.6 μm gap between electrodes. The gap is transmissive, with a refractive index dependent on the voltages applied to adjacent pixel electrodes. The beam from a Ti:sapphire oscillator (KM Labs), with 40 nm optical bandwidth centered at 790 nm, is collimated to $2w_{\text{in}} \approx 4$ mm diameter and sent into the shaper. For the prism implementation, we used a 750 mm focal length lens and an SF10 Brewster prism. The spectral focus is $2w_0 \approx 190$ μm or 118 pixels. In the grating version, a 600 mm^{-1} grating is used with a 200 mm focal length lens. The spectral focus is $2w_0 \approx 50$ μm or 31 pixels. The SLM reflectivity is measured to be 93% and the total shaper efficiencies are 77% and 35% for the prism and grating shapers, respectively, although higher throughput should be possible with anti-reflection coated optics and a grating optimized for efficiency. As with any Martinez stretcher, initial quadratic spectral phase on the input pulses can be compensated for by adjustment away from the $4f$ condition. We found it more convenient to use a single-prism compressor [13] placed after the pulse shaper to compensate residual chirp from the oscillator output. This preserves the maximum dynamic range of SLM phase for pulse shaping. To characterize the pulse shaper, we use a spectral interferometry technique described below. Temporal pulse measurements in this paper are performed with a second harmonic generation frequency resolved optical gating (SHG-FROG) device [14], making use of a high-speed principal component generalized projection (PCGP) phase retrieval algorithm [15].

#84226 - $15.00 USD Received 20 Jun 2007; revised 28 Jun 2007; accepted 29 Jun 2007; published 5 Jul 2007

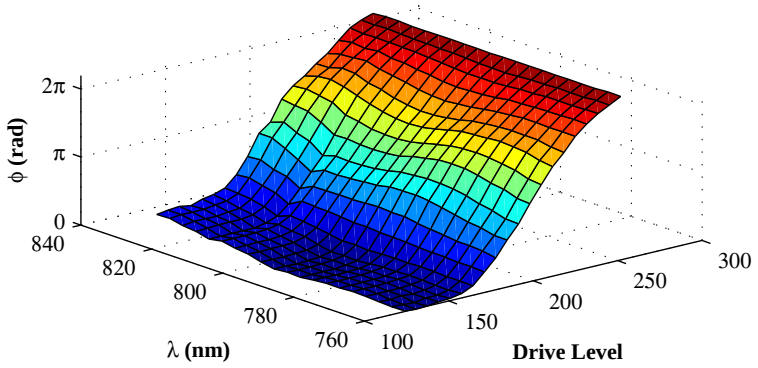

Fig. 1. Calibration of phase ϕ with respect to wavelength λ and drive level. Surface mesh lines are shown to enhance visualization of surface curvature; actual data is collected at higher resolution.

2. Calibration

As with any pulse shaping device, an accurate calibration is critical for producing predictable pulse shapes. Here we describe the procedure for characterizing the phase response of the LC-SLM, yielding a functional mapping from wavelength to pixel, and drive voltage to phase. We then proceed to analyze phase gratings for amplitude shaping, establishing an optimal grating spatial frequency f_g and calibrating depth of modulation Δ to transmission T.

2.1. Phase calibration

To calibrate the device we first find the relationship between pixel and frequency by sweeping a π–phase step across the SLM and observing the dip in the transmitted spectrum due to the phase discontinuity. We fit a quadratic curve to these data, and from the first-order coefficient of this fit we empirically estimate $\alpha \approx 28$ mm rad^{-1} fs for the prism shaper, and $\alpha \approx 44$ mm rad^{-1} fs for the grating shaper; both agree well with the theoretical values of $\alpha \approx 26$ mm rad^{-1} fs and $\alpha \approx 44$ mm rad^{-1} fs, respectively calculated from the optical dispersion of the prism or grating. Next, we make use of an inline spectral interferometry technique [16], where a birefringent crystal splits the input pulse into two time delayed pulses with orthogonal polarizations. The LC-SLM only shapes one of the polarizations, leaving the second as a reference. A polarizer at 45° projects the two pulses to the same polarization and the resulting interference fringes are measured with a spectrometer (OceanOptics). Here the phase difference between the pulses is very stable, leading to more reliable phase measurements than by use of a Mach-Zehnder interferometer. We then extract the phase difference with a Fourier sideband filtering algorithm [17]. We calibrate the drive voltage to phase by running all the SLM pixels through their drive range, measuring interference fringes, and computing the resulting imparted phase. Figure 1 shows this calibration for the prism shaper; results are similar for the grating case.

2.2. Amplitude calibration

Armed with a reliable phase calibration, we characterize the amplitude control afforded by our approach. Applying a range of phase gratings, we establish an optimal $f_g = 27$ mm^{-1} for the prism-based shaper, and $f_g = 60$ mm^{-1} for the grating-based shaper. We find that for both setups the optimal phase grating period is approximately $2w_0/5$. The spatial frequency is high enough that the grating diffracts light outside of the aperture of the apparatus, yet low enough

#84226 - $15.00 USD Received 20 Jun 2007; revised 28 Jun 2007; accepted 29 Jun 2007; published 5 Jul 2007

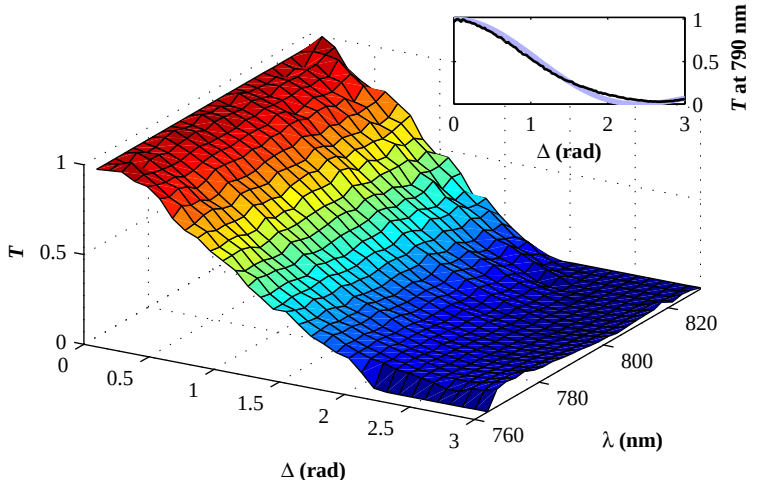

Fig. 2. Measured transmission T, plotted with respect to increasing phase grating depth Δ, as applied across the entire phase mask. Surface mesh lines are shown to enhance visualization of surface curvature; actual data is collected at higher resolution. Inset: line-out of the above plot at 790 nm, showing transmission T with respect to the phase grating depth (black line). Theoretical curve (light blue line) shown for comparison.

that the discreteness of the SLM has a negligible impact. We measure transmission T as the ratio of shaped/unshaped spectral intensity, observed from the shaper output. Figure 2 shows T across the measured spectrum for a 62-μm period sinusoidal phase grating on the prism-based shaper, varying Δ. The inset shows T at 790 nm (black line), which agrees very favorably with the $|J_0(\Delta)|^2$ dependence (light blue line) predicted theoretically by Eq. (3). In this case, the maximum attenuation at the center wavelength is 97%.

3. Pulse shapes

The above calibration allows the generation of arbitrary pulse shapes with specified amplitude and phase. For best results, we first remove the residual spectral phase distortion present after the prism compressor. To accomplish this, we measure a FROG trace with the mask set to constant zero phase, and retrieve the phase with the PCGP algorithm. The inverted phase is added to the shaper mask to obtain near-transform-limited 28 fs pulses, verified by another FROG measurement. The ability to compress pulses by measuring a spectral phase and applying its inverse with the SLM validates both our calibration and pulse measurement techniques.

We demonstrate the phase shaping capabilities of the pulse shaper, independent of amplitude, by applying a sinusoidal and then a V-shaped spectral phase. In the case of sinusoidal phase, we measure the imparted phase with the aforementioned spectral interferometry method, and compare the results to the intended phase mask. Figure 3 shows excellent fidelity in producing this phase. In the case of a V-shaped spectral phase, the halves of the spectrum see a linear phase with slope τ, with opposite signs on each half. The effect is to split the pulse into a pair, separated in time by 2τ. Results for $2\tau = 400$ fs are shown in Fig. 4. The observed spectral modulations here are due to scattering at the 2π phase wrapping points.

For amplitude shaping, we first observed the effects of phase gratings with finite width across the mask, and then produced a temporal sinc^2 intensity profile by shaping the spectrum into a square. We applied a finite-width phase grating, centered at 790 nm, to produce spectra with

#84226 - $15.00 USD Received 20 Jun 2007; revised 28 Jun 2007; accepted 29 Jun 2007; published 5 Jul 2007

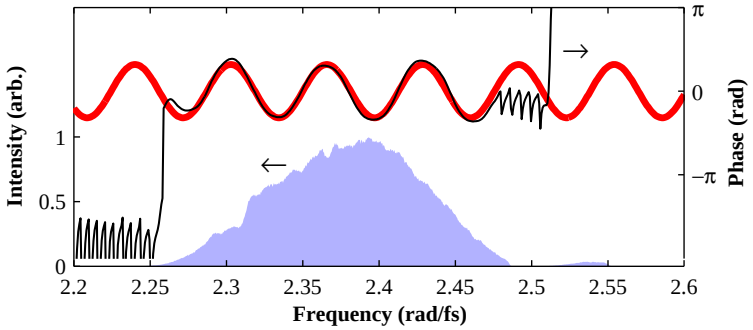

Fig. 3. Verification of phase calibration by applying a low-frequency sinusoidal spectral phase. Spectral intensity (light blue patch), applied phase mask (red line), and phase as measured by spectral interferometry (black line).

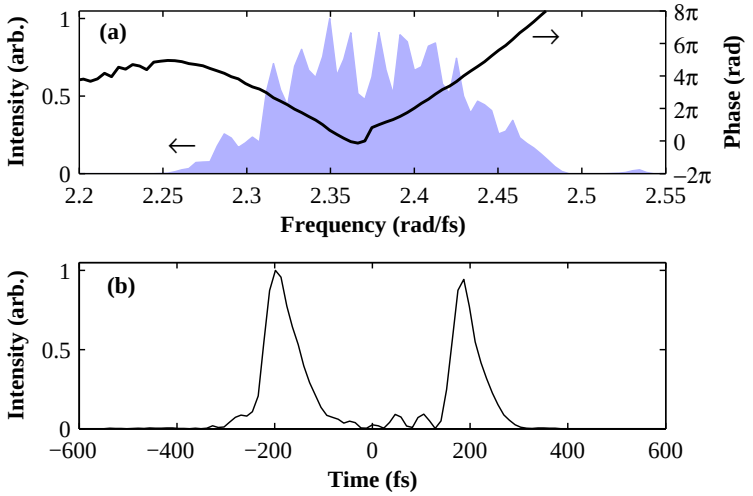

Fig. 4. (a) Measured spectral intensity (light blue patch) and phase (black line) for splitting a pulse into a delayed pair. (b) Temporal intensity, showing separation of 400 fs.

#84226 - $15.00 USD Received 20 Jun 2007; revised 28 Jun 2007; accepted 29 Jun 2007; published 5 Jul 2007

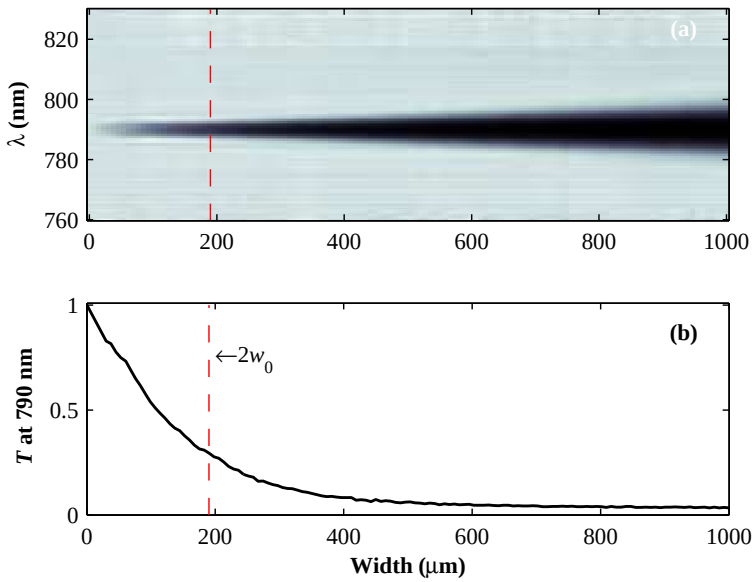

Fig. 5. Spectral notch of increasing width. (a) Measured spectra, normalized by the first spectrum, showing increased attenuation and broadening of notch as phase grating width is increased. (b) Transmission T at 790 nm, showing increase in attenuation which levels off when the phase grating is wider than the spectral focus $2w_0$, marked by the red dashed line.

a notch in the center. We proceeded to broaden the notch by widening the phase grating. Figure 5(a) shows the measured output spectra, normalized by the unmodulated spectrum, as a phase grating of increasing width is applied to the center of the spectrum. For phase grating widths $< 2w_0$, the notch is as wide as the spectral focus and increases in attenuation until the width is comparable to the spectral focus, and then the notch begins to broaden to cover more frequencies. The plot in Fig. 5(b) shows the relative reflected intensity recorded by the spectrometer at a wavelength of 790 nm. As expected, the attenuation plateaus once the phase grating width is on order of the spatial mode size in the Fourier plane. Next we produce a square-shaped spectrum, as shown in Fig. 6(a). The mask attenuates frequencies outside the desired square, and is set to nearly flatten the top of the spectrum. Since the inverse Fourier transform of a square spectrum is a sinc function, the intensity profile of such a pulse is a sinc^2, with alternating π phase, in good agreement with the retrieved pulses shown in Fig. 6(b).

Finally to demonstrate simultaneous control over spectral phase and amplitude, we shaped the spectrum into two lobes separated by 0.08 rad/fs and shifted the relative phase ϕ between the lobes. The spectral lobes interfere in the time-domain in a manner analogous to a double-slit experiment. The inset in Fig. 7 shows the measured FROG traces (left half), with the PCGP retrieved traces (right half). The resulting pulse shape intensity profile (blue patches) lies within a region identified in Fig. 7 with a Gaussian envelope (red lines), shown as a visual guide. The intensity modulation period is set by the separation of the spectral peaks and agrees with the expected ~ 80 fs period. The temporal intensity interference structure shifts in the expected manner with the application of a relative phase between the two spectral lobes.

#84226 - $15.00 USD Received 20 Jun 2007; revised 28 Jun 2007; accepted 29 Jun 2007; published 5 Jul 2007

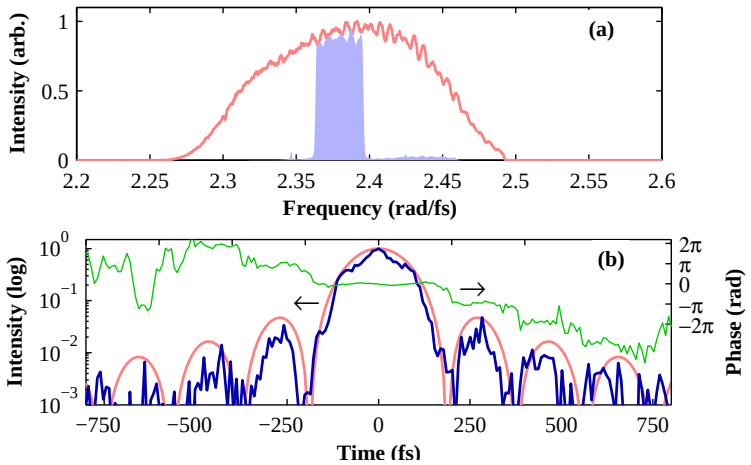

Fig. 6. Amplitude-only shaping. (a) Unshaped (red line) and shaped (light blue patch) square spectrum. (b) Resulting temporal profile (blue line), with a sinc^2 (red line) for comparison. Spectral phase (green line) shows π phase offset between adjacent lobes.

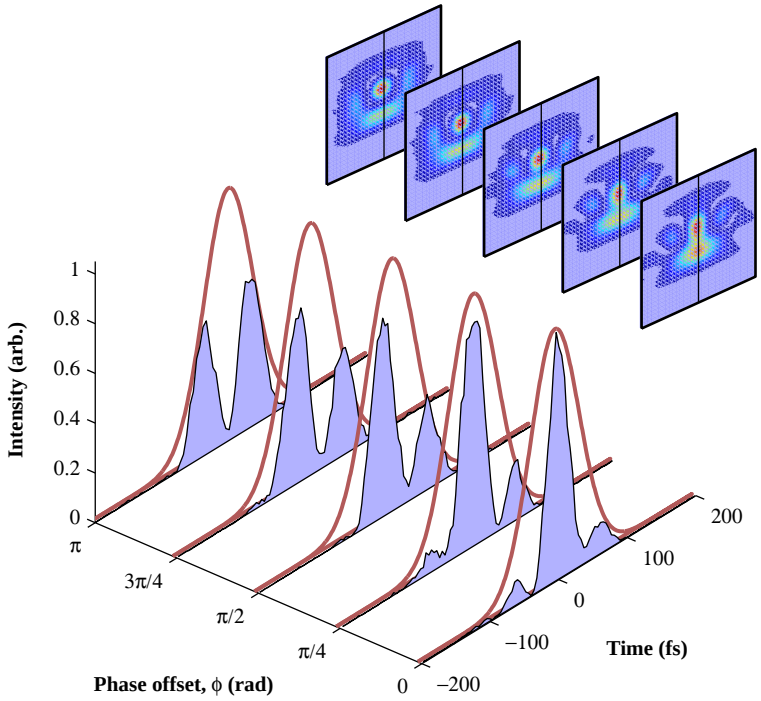

Fig. 7. Temporal profiles for the spectral double-slit experiment. Inset: FROG traces depict both measured (left half of trace) and numerically reconstructed (right half) traces.

#84226 - $15.00 USD Received 20 Jun 2007; revised 28 Jun 2007; accepted 29 Jun 2007; published 5 Jul 2007

4. Summary

In summary, we have demonstrated simultaneous amplitude and phase control of ultrafast laser pulses using a single linear LC-SLM. The amplitude shaping is made possible by over-sampling each spectral focus and writing a phase grating with sufficiently high frequency, a technique that can be extended to temporally shape octave-spanning spectra. The close pixel spacing, large number of pixels, and small footprint of the SLM used here enables this simple and compact design. Moreover, the high reflectivity of the SLM also results in a highly efficient pulse shaper when a prism is used for the angular dispersive element. This pulse shaper design is anticipated to find wide-spread use due to high efficiency, cost-effectiveness and compactness with amplitude and phase shaping capability suitable for use with mode-locked oscillator pulse trains.

Acknowledgments

We would like to thank Steve Serati, Anna Linnenberger, and Kelly Gregorak of Boulder Nonlinear Systems in Lafayette, CO for their collaboration and providing the SLM. The authors also gratefully acknowledge support from the NSF CAREER Award ECS-0348068, ONR Young Investigator Award, the Beckman Young Investigator Award, and Sloan Research Fellowship support for R.A.B.

#84226 - $15.00 USD Received 20 Jun 2007; revised 28 Jun 2007; accepted 29 Jun 2007; published 5 Jul 2007